Real-time Broadband RFI Excision for the Upgraded GMRT

Ruta Kale, Kaushal D. Buch, Sanjay Kudale, Mekhala Muley, Ajith Kumar B.

March 4, 2020

Contents

1   Introduction

Radio Frequency Interference (RFI) mitigation is a major challenge for all the radio observatories across the world. It adversely affects the radio observations making it difficult to achieve the theoretical sensitivity and can create signal distortion if not mitigated early in the processing chain. Over the years, a wide range of mitigation techniques have been proposed at different locations in the receiver system of a radio telescope [1, 2].

Two broad strategies to mitigate RFI are: i) offline method: after the data (visibilities or beam) has been recorded and ii) online method: on-the-fly at the highest possible time resolution before it is processed or recorded in the final form accessible to the user. In the online mitigation, one does not record the "raw" form of the data on which the mitigation happens and thus there is permanent loss of the samples that are selected for excision. On the other hand, offline methods are inadequate as they generally operate on data recorded at time resolution much coarser than Nyquist sampling. This limits their capability to excise the RFI as compared to the online methods. The online methods can do much damage control with a lower amount of flagging.

A real-time broadband RFI mitigation system has been developed for the Upgraded GMRT (uGMRT) [3, 4]. Here, we report the engineering, imaging, and beam/pulsar results from the test observations in all the bands of the uGMRT during the monsoon of 2018 and 2019. Broadband power-line RFI is almost always present in uGMRT bands 2 (120 - 240 MHz), 3 (300 - 500 MHz) and 4 (550 - 850 MHz) but the monsoon period is chosen to understand the performance in the worst RFI situations arising due to increase in the wind-speed and moisture.

1.1   RFI at the uGMRT

In terms of its frequency-domain characteristics, RFI can be categorized as Broadband (BB) or Narrowband (NB). In the time-domain, BB RFI manifests as short duration, impulsive bursts of interference signal, typically from spark-like events (e.g. lightning discharge, power line discharge, spark ignition discharge); whereas NB RFI is due to spectrally-confined sources such as transmissions from communication systems - terrestrial or otherwise. Example of uGMRT band-3 data affected by NB and BB RFI is shown in Fig. 1. The broadband RFI is highlighted with boxes.

BB RFI is stronger at low frequencies (below 1 GHz) and hence its excision is important for observing in bands 2, 3 and 4 of the uGMRT. Details of power-line RFI at GMRT and need for mitigation from an earlier study are described in the reports [5, 6]. Of particular interest to this work is that these reports describe the power-line RFI and its effect on the GMRT observations along with various measurements carried in and around the array. It also describes the harmful levels of interference, affect on the sensitivity due to power-line RFI with an emphasis on the need for RFI mitigation.

1.2   Need for real-time excision

1. For temporally impulsive RFI (Fig. 2), the total energy spreads in the Fourier domain and hence excision is needed before Fast Fourier Transform (FFT) stage. Power-line RFI has a low duty cycle but a high spectral occupancy and hence a frequency selective filter (like notch or band-stop) does not work for this case.
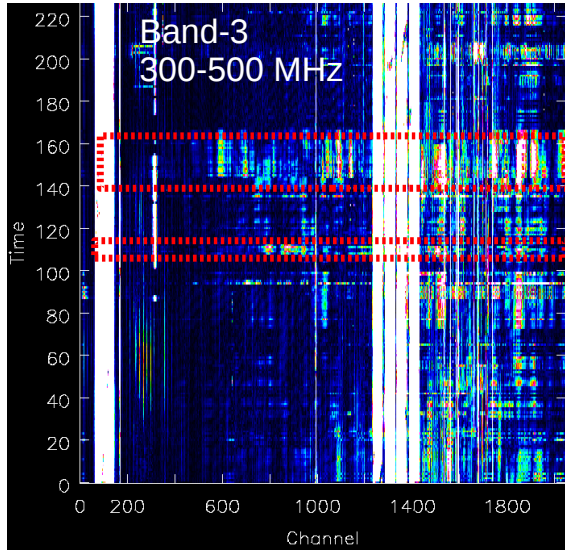
Figure 1: The time-frequency plane data from the uGMRT at band 3 for a baseline between central square antennas is shown. A couple of examples of BB RFI are marked by the red dashed boxes. The lowest channel number is at the highest frequency.
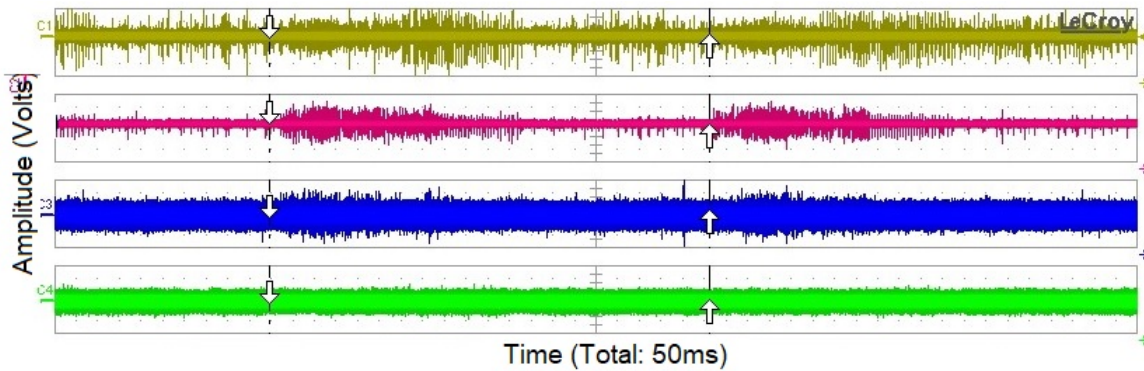

Figure 2: A typical example of uGMRT band-2 (C01 antenna, first subplot), band-3 (C02 antenna, second subplot), band-4 (C05 antenna, third subplot) and band-5 (C08 antenna, fourth subplot) data acquired simultaneously at the input of GWB (100 MHz bandwidth) using a 4-channel mixed-signal oscilloscope with 5ns sampling; 50ms data shown in the plot (X-axis: Time (20.33ms between the dotted markers),Y-axis: Voltage, 500mV/division for band-2 and band-3 100mV/division for band-4 and 1V/division for band-5). The periodically repeating impulses are from the power-line interference.

3

2. RFI is correlated in closely-spaced antennas and hence excision is best suited in the pre-correlation domain. This is especially important as the GMRT array has closely spaced antennas in the central square.

2 Online BB RFI Mitigation for the uGMRT

BB RFI is dominant at lower frequencies (<1GHz) and occurs due to gap discharge or corona discharge on high-power transmission lines and associated transmission equipment in the vicinity of the GMRT array. The online (real-time) BB RFI filter for the GMRT Wideband Backend (GWB) operates on digitized (8-bit signed integer) time-domain Nyquist-sampled signal on Field Programmable Gate Array (FPGA) [7]. The statistical estimation of the signal is carried out using Median-of-MAD (MoM) estimator. There are two detection techniques available: (a) Voltage detection and (b) Power detection. The filtering (replacement) options available are digital noise, constant value and threshold. In this report, the voltage detection and the results using this technique are described.

Median Absolute Deviation (MAD) is computed on Nyquist-sampled digitized time series for each antenna and polarization ($MAD = median(abs(X_i - median(X)))$) on 16k data samples. To get a more robust estimation, median of 16k MAD values is computed for getting Median-of-MAD (MoM). To meet the real-time requirements, this estimation is carried out on every fourth input sample out of the samples arriving at 1.25ns interval. (Calculation: ($16384 samples * 16384 MAD values * 1.25 * 10^{-9} sampling period$) * $4 = 1.34s$). Thus, 1.34s worth of data goes in to the real-time statistics for the RFI filtering and is applied to the subsequent data. Values outside the threshold $median \pm n * 1.4826 * MoM$ are treated as RFI and are replaced either by constant value or digital noise or the threshold value. n is kept as 3 for a 3σ threshold.

RFI counter keeps a record of the number of detected RFI samples and total number of samples per antenna and polarization. The ratio of these counts would provide the fraction of flagged samples over user-defined time intervals (minimum duration of 5 minutes as per current configuration) during the observation. Example of processed data from the counter output is shown in Section ??.

2.1 Testing scheme for the real-time RFI filter: System setup and configuration

Table 1: The set up in 1:2 mode.

Unfiltered	C00	C02	C04	C06	C09	C11	C13	E02	E04	E06	S02	S04	W01	W03	W05
AIPS no.	01	03	05	07	09	11	13	15	17	19	21	23	25	27	29
Filtered	C01	C03	C05	C08	C10	C12	C14	E03	E05	S01	S03	S06	W02	W04	W06
AIPS no.	02	04	06	08	10	12	14	16	18	20	22	24	26	28	30

The quality of RFI filtering was tested through a comparative analysis between unfiltered and filtered signals of the same antenna for the same instance of time. This scheme was implemented by configuring the antenna input and the corresponding GWB parameters to support simultaneous processing for the same antenna signal through two chains one with the RFI filter and one without.

Data for imaging tests were taken with the mode of *digitalcopy*. In this mode signals from half the antennas were digitally copied (inside the FPGA) into the rest half. One set was passed through the filter and the unfiltered copy was obtained in the signals from the other set of antennas. The schematic of this is shown in Fig. 3. The mode is referred to as 1 : 2 digital copy mode. The mode where the online RFI
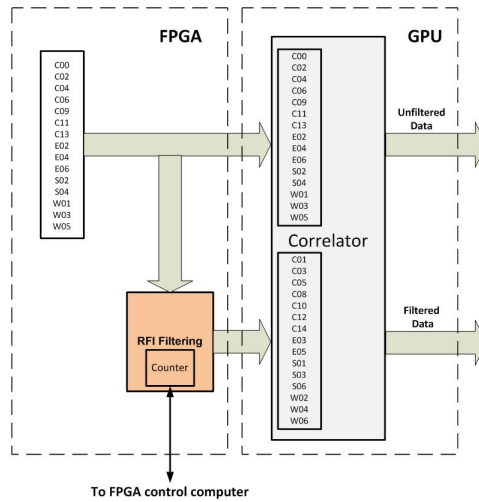
Figure 3: GMRT antenna configuration in the 1:2 digital copy mode. In this mode signals from half the antennas are copied into the rest half. One set passes through the filter and the unfiltered copy is obtained using the signals from the other set of antennas.

filter was used on all the antennas without retaining a copy of the unfiltered signal is referred to as $1:1$. For each observation the counter values were recorded to provide an estimate of the number of samples affected by the RFI excision. All the test described in this report have been carried out using the 1:2 digital copy mode.

For the imaging tests, the filtered and unfiltered data were recorded in the same long-term accumulation (.lta) file and then converted to FITS format using the standard *listscan* and *gvfits* programs. The names of the antennas that were filtered and unfiltered were provided in the log file produced by *listscan* and separate FITS files were created for further analysis. Table 1 provides antenna names for which the filtered and unfiltered copy of the signal is present. The AIPS antenna IDs are also given for reference. Data analysis was carried out using the NRAO Astronomical Image Processing System (AIPS) and Common Astronomy Software Applications (CASA).

3 Results from engineering tests

We carried out tests in the monsoon of 2018 and 2019, primarily in the uGMRT bands-3 and 4 over RF bandwidth of 200 MHz to understand the effect of RFI filtering on the beam and interferometer outputs.

An example of engineering test carried out on 26 July 2018 in Band-3 is presented. The test was carried out using the 1:2 filtering mode on 3C147 and a processing bandwidth of 200 MHz. Beam and interferometer data were recorded simultaneously at a time-resolution of $81.92\mu s$ and 671ms respectively. The plots are for a single spectral channel corresponding to 451 MHz. This spectral channel has expected power level and is away from the channels affected by NB RFI. The cross-correlation function, closure phase, beam and beam-FFT, and percentage flagging are described.

3.1 Effect on closure phase

The filtered and unfiltered copy of a single spectral channel time series for a 3σ threshold and digital noise replacement is shown. Fig. 4 shows the closure phase between three closely spaced antennas of the central square (C02,C06 and C09) for unfiltered and filtered outputs. The first three subplots show the cross-correlation amplitude for three baselines. Subplots 4,5 and 6 show the phase of the cross-correlation. The closure phase computed from the data in subplots 4,5 and 6 is shown in subplot 7. RFI causes fluctuations in the closure phase up to about ± 60 degrees which is brought close to zero (within ± 5 degrees) in the filtered data.
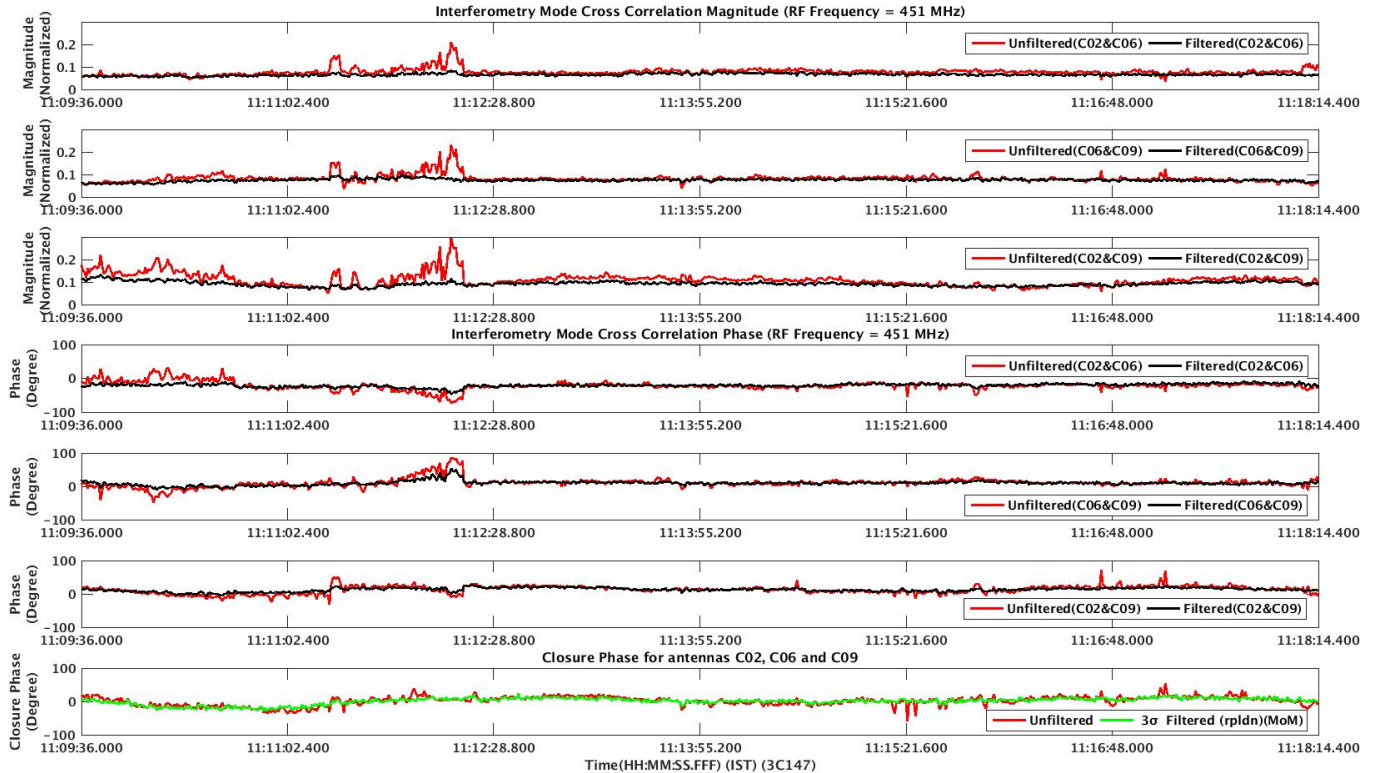

Figure 4: Closure phase comparison between antennas C02,C06 and C09. The closure phase computed from the data in subplots 4,5 and 6 is shown in subplot 7. In this case, RFI causes error in the closure phase up to ± 60 degrees which is reduced to zero (within ± 5 degrees) in the filtered data. [Sec. 3.1]

3.2 Effect on the Cross-correlation function (CCF)

Presence of BB RFI causes larger fluctuations in the measurement of the cross-correlation function. This is particularly prominent on shorter baselines (The central square and a few arm antennas) where the RFI between the antennas is correlated. Fig. 5 shows that the ratio of standard deviation of unfiltered to filtered data is in the range of 1.5 to 3. It can be seen where there was no BB RFI, the error bar has been unaltered by the filtered output (see C09-E06 baseline for channel-II in the Fig. 5).
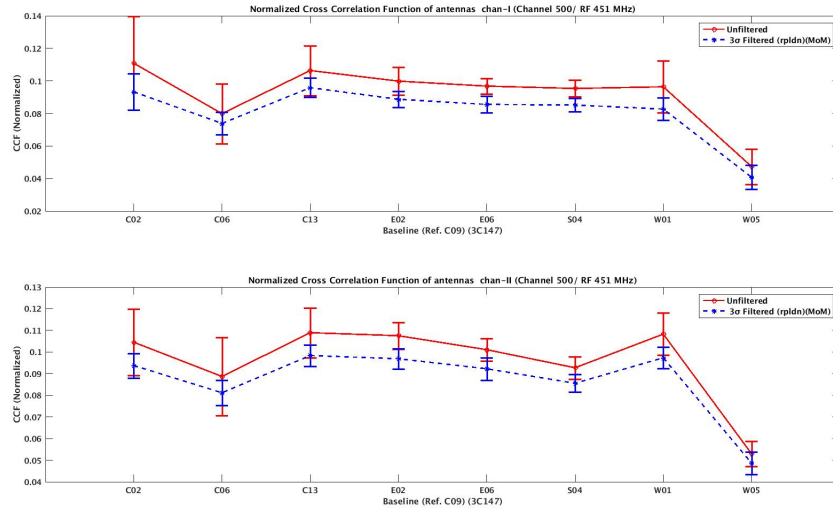
Figure 5: CCF comparison between antennas with reference to C09 antenna. The ratio of standard deviation of unfiltered to filtered data is in the range of 1.5 to 3. It can be seen where there was no BB RFI, the error bar has been unaltered by the filtered output (see C09-E06 baseline for channel-II). [Sec. 3.2]

3.3 Simultaneous beam and interferometer comparison

Time-series of single spectral channel show improvement between the unfiltered and filtered beam data in subplot 1 of Fig. 6. The simultaneous cross-correlation amplitude (subplot 2) and phase (subplot 3) show that both the quantities remain stable while their unfiltered counterparts fluctuate during event of BB RFI. A maximum improvement of 7.7 dB (ratio of unfiltered to filtered value) is observed in the beam data shown in subplot 1.

3.4 Beam data analysis

Time-series of single spectral channel beam data is shown in subplot 1 of Fig. 7. The second subplot shows the Fourier transform of this time-series. The 50 Hz, 100 Hz, and harmonics are clearly seen in the unfiltered data which are significantly removed in the filtered data set. These harmonics correspond to the multiples of the 50 Hz power-line frequency. The power in the 50 Hz and 100 Hz frequency goes down by a factor of four for the filtered data.
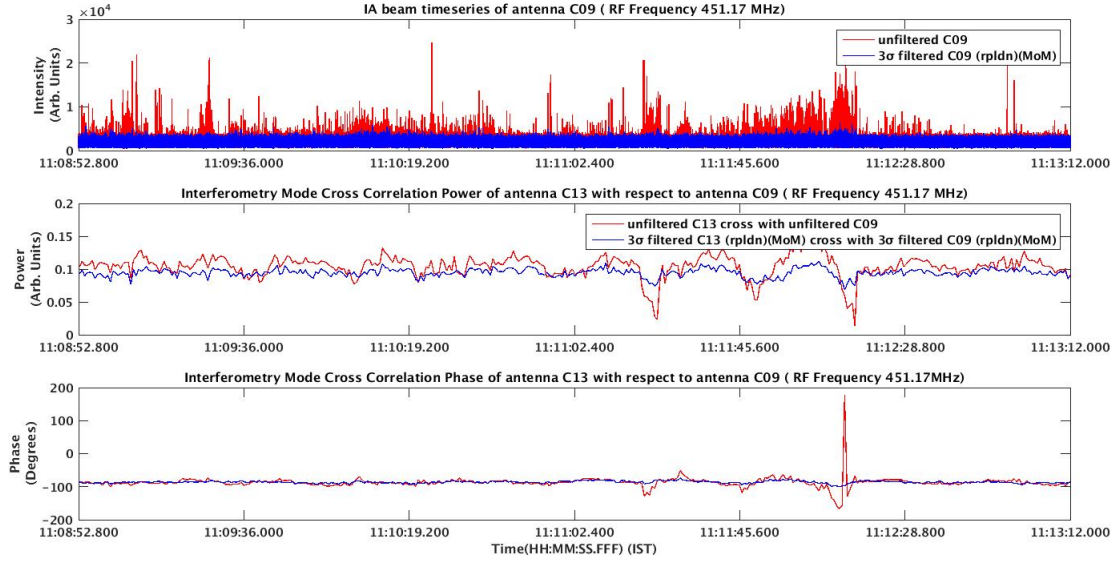
7

Figure 6: Comparison between beam and interferometry simultaneous observation. The simultaneous cross-correlation amplitude (subplot 2) and phase (subplot 3) show that both the quantities remain stable while their unfiltered counterparts fluctuate during event of BB RFI.A maximum improvement of 7.7 dB (ratio of unfiltered to filtered value) is observed in the beam data shown in subplot 1. [Sec. 3.3]

3.5 Antenna-based percentage flagging

Total fraction (in percentage) of samples replaced during this test for each antenna and polarization are shown in Fig. 8. This is generated from the counters within the FPGA design. For this test observation,the average RFI excised is less than 2%. It is noted that the flagging percentage can differ significantly between the two polarizations of the same antenna.
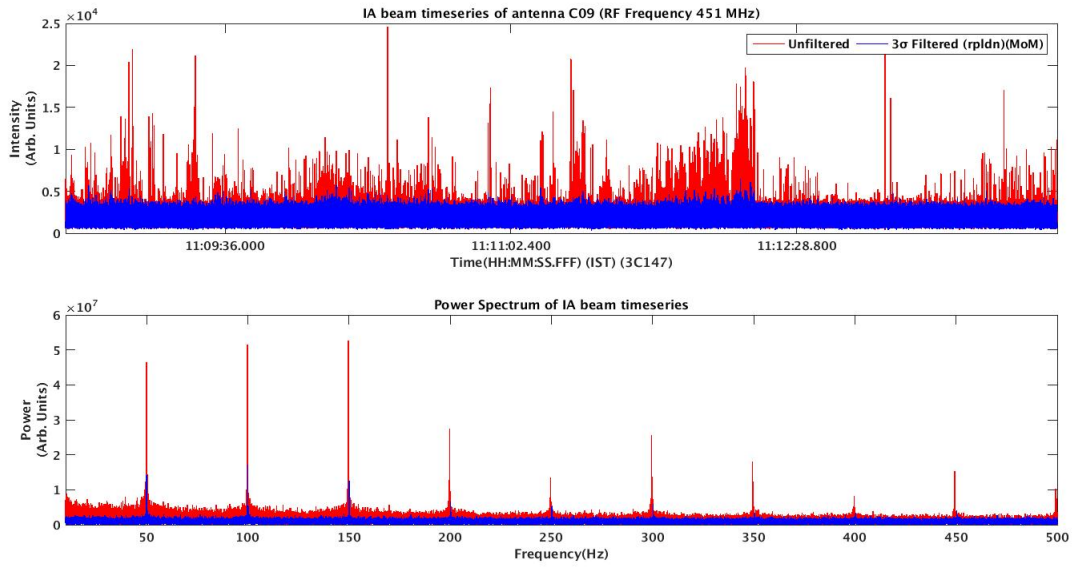
Figure 7: Single spectral channel beamformer output and its Fourier transform. The 100 Hz, 200 Hz and harmonics are clearly seen in the unfiltered data which are reduced by a factor of two (100 Hz) and four (200 Hz) in the filtered data set. These harmonics correspond to the multiples of power-line frequency (50 Hz). [Sec. 3.4]
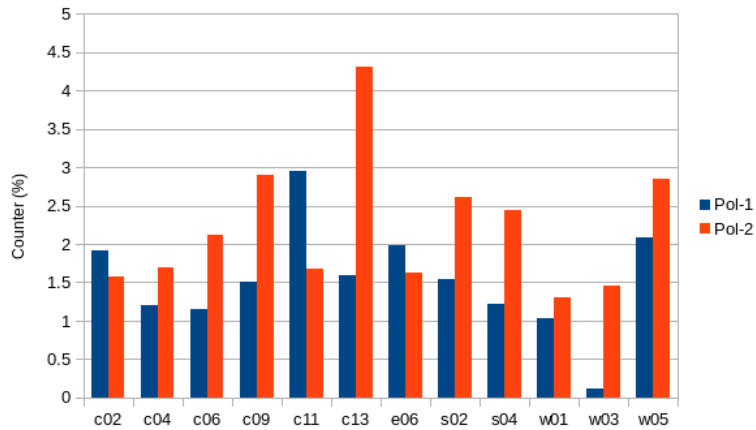

Figure 8: Bar chart showing the percentage fraction of RFI samples detected and replaced during the observation. In this case, the average RFI excised is less than 2%. [Sec. 3.5]

4 Beamformer data analysis and Pulsar observations

4.1 3C48

As part of the engineering tests, 3C48 was observed at Band-4 on 14 June 2018. The observations were carried out in the 1:2 digital copy mode with voltage technique (3σ threshold). The effect of BB RFI filtering was observed using the GMRT Pulsar Tool (*gptool*).

As an example, two blocks from the observation of 3C48 are shown with the unfiltered and filtered counterparts (Fig. 9, 11 and Fig. 10, 12). In order to isolate and find out the effect of real-time BB filtering, the RFI filtering within the *gptool* was disabled and the processing was done with zero Dispersion Measure (DM) settings. It can be seen that the bursts of interference (which are broadband in nature) have been completely removed in the filtered data.
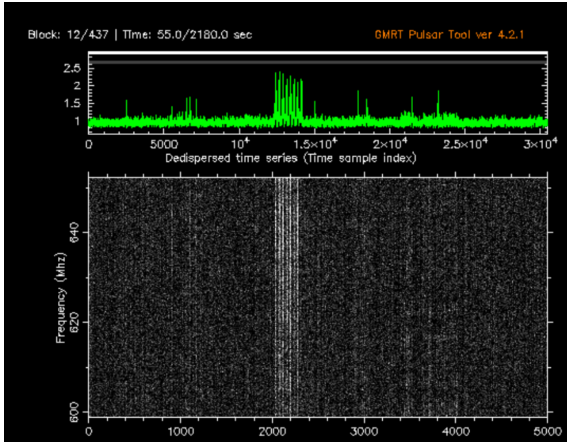

Figure 9: Beamformer mode for 3C48(unfiltered copy): observation carried out in the digital copy (1:2) mode.
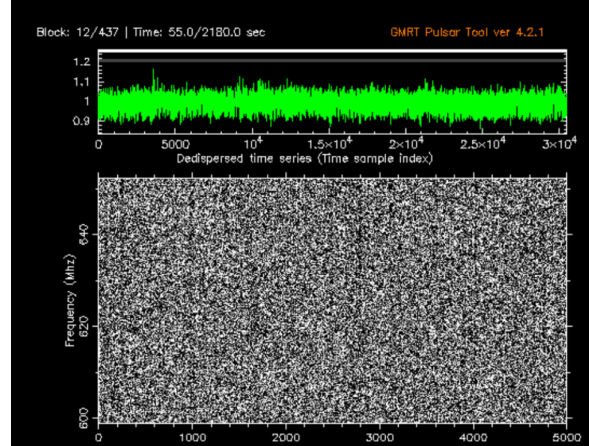

Figure 10: Beamformer mode for 3C48 (filtered copy): observation carried out in the digital copy (1:2) mode.
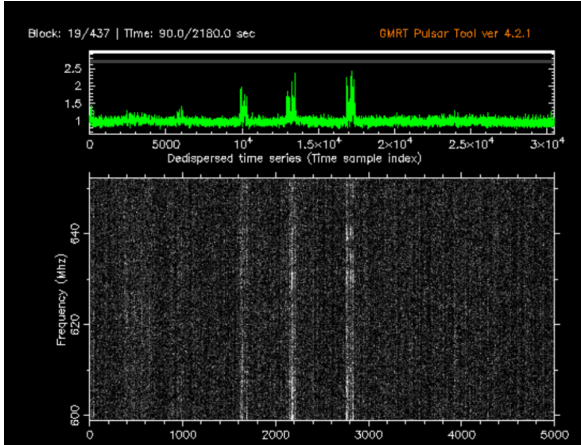

Figure 11: Beamformer mode for 3C48(unfiltered copy): observation carried out in the digital copy (1:2) mode.
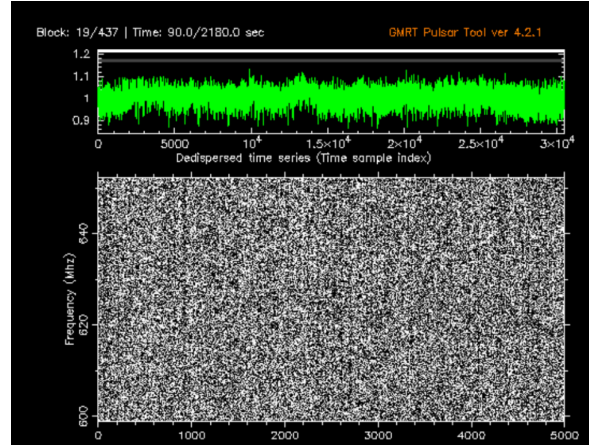

Figure 12: Beamformer mode for 3C48 (filtered copy): observation carried out in the digital copy (1:2) mode.

4.2   PSR B0329+54 and PSR J0418-4154

Pulsar observations were carried out in the incoherent array (IA) mode on 5th July 2019 at Band-3. Two pulsars B0329+54 and J0418-4154 were observed during this session. The purpose of this test was to check the effect of filtering on strong single pulses and on averaged folded profiles. The observation was carried out with 14 antennas in the 1:2 digital copy mode and with RFI filtering in the voltage detection mode at 3-sigma threshold and replacement by digital noise. The bandwidth was 200 MHz in 300-500 MHz band with 4096 spectral channels and a time-resolution of 327.68 μs.

The de-dispersed time-series from a strong pulsar B0329+54 shows an improvement of SNR by a factor of 4 (Fig. 14) over the unfiltered version (Fig. 13). The SNR of unfiltered is 60 which increases to 240 after filtering.
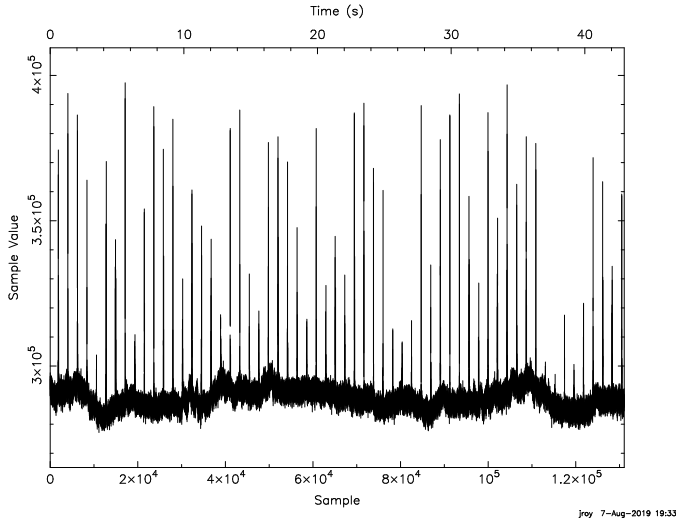

Figure 13: Unfiltered de-dispersed time-series from a strong pulsar B0329+54 : observation carried out in the digital copy (1:2) mode.
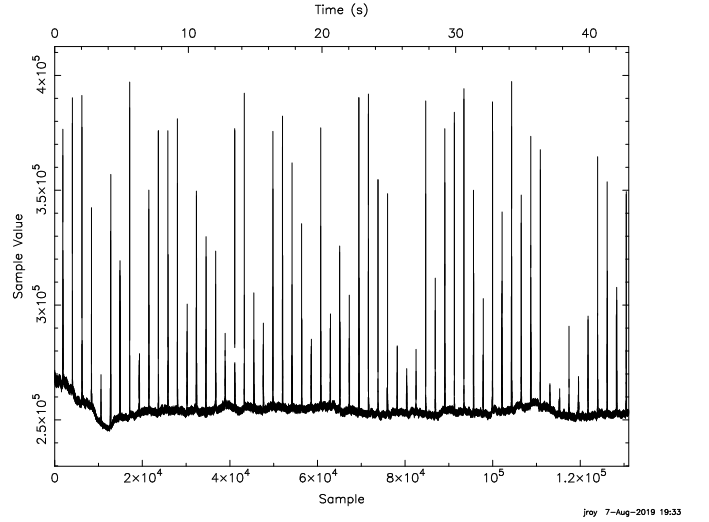
Figure 14: Filtered de-dispersed time-series from a strong pulsar B0329+54 : observation carried out in the digital copy (1:2) mode. SNR improvement by a factor of 4.

The strong single pulse from PSR B0329+54 seems to have not clipped during filtering (Fig. 15 and Fig. 16). These are initial results and a detailed analysis will be carried out to quantify if there is any change of profile shape by filtering.
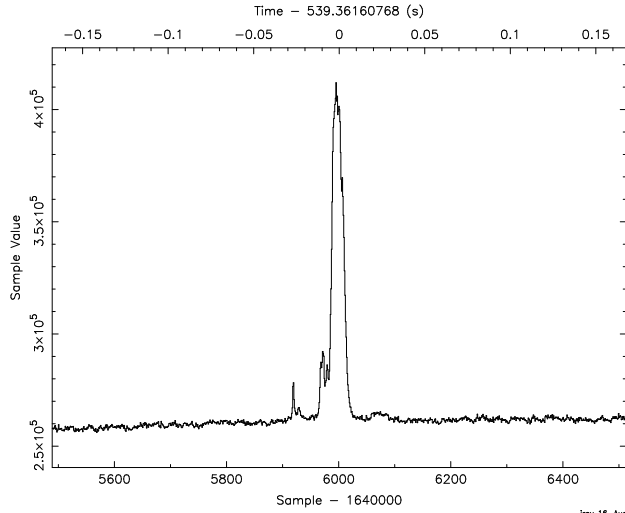
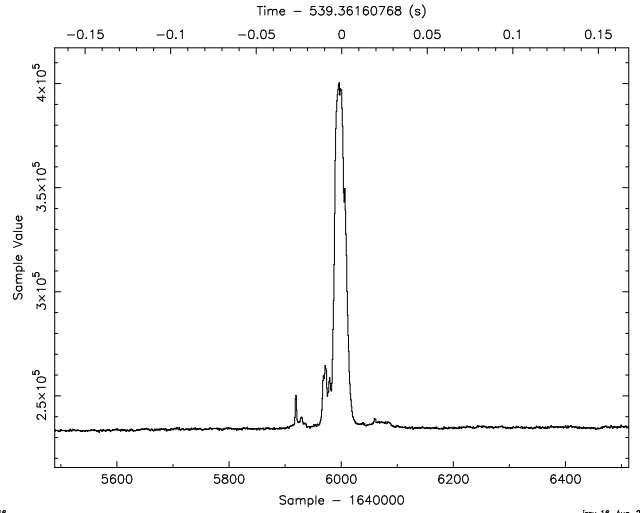Figure 15: Single pulse (unfiltered) from a strong pulsar B0329+54

Figure 16: Single pulse (filtered) from a strong pulsar B0329+54.

Similar observation on PSR J0418-4154, a much weaker one than B0329+54 (by three order of magnitudes) also shows similar improvement in the mean SNR of the folded profile (Fig. 17 and Fig. 18).
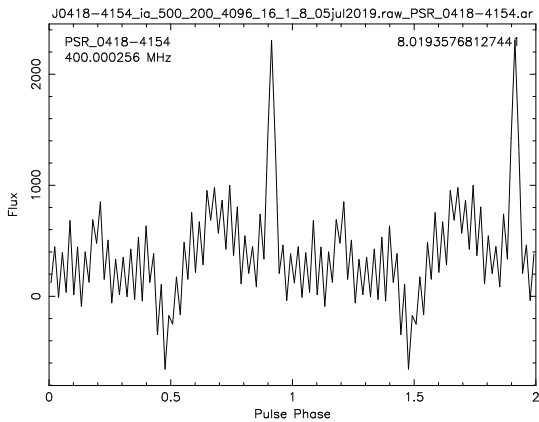

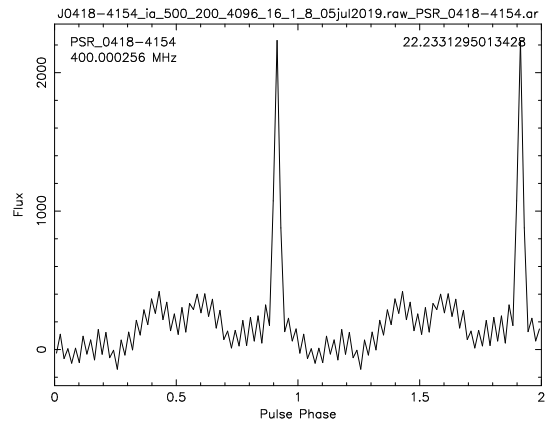Figure 17: Unfiltered profile of PSR J0418-4154.

Figure 18: Filtered profile of PSR J0418-4154. Three orders of improvement in the SNR of the folded profile.

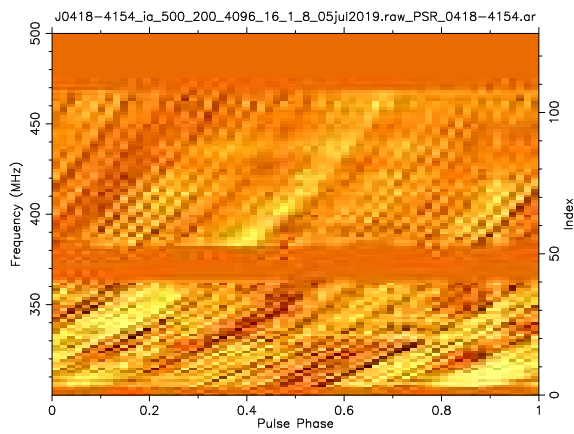The frequency-phasogram is also much cleaner for the filtered data (Fig. 19 and Fig. 20).

12

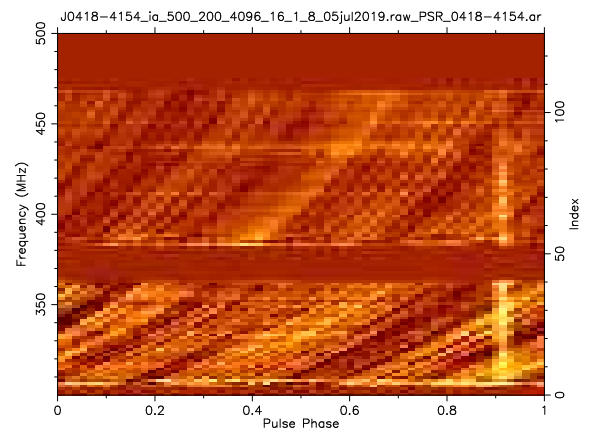Figure 19: Unfiltered frequency-phasogram for PSR J0418-4154.

Figure 20: Filtered frequency-phasogram for PSR J0418-4154.

5 Results from interferometric mode tests

A summary of the tests in the interferometric mode is provided in Table 2.

Table 2: Summary of the imaging tests using the voltage detection method for online RFI excision.

Date	Band (Freq.)	Mode	Sources	Time (min)
14 Jun. 2018	4 (610 MHz)	1:2	3C48	20
11 Sept. 2018	2 (150 MHz)	1:2	0319+415(3C84),0432+416, 3C48	80, 20, 10
11 Aug. 2019	3 (330 MHz)	1:2	A2744, 0116-208, 3C48	180, 35, 20
13 Aug. 2019	4 (610 MHz)	1:2	A2744,0116-208, 3C48	240, 45, 30
09 Sept. 2019	5 (1400 MHz)	1:2	3C147	35

5.1 Effect of filtering on the visibilities

In this section, results from the test in 1:2 mode at band 4 (14 June 2018) are described as an example of the differences expected in data with and without filtering. The data for this test were analysed in AIPS. The filtered and unfiltered data were processed in identical manner.

5.1.1 UV-distance and frequency

In Fig. 21, the calibrated amplitude is plotted as a function of uv-distance for the channel 200. The difference due to the filter is mainly evident at the short baselines where the number of outlier points in unfiltered data are seen. The time-frequency plane with amplitude plotted as grey-scale is shown in Fig. 22. NB and BB RFI are both seen and the effect on one broadband feature is highlighted. An example of uncalibrated spectrum is shown in Fig. 23. The two polarizations are shown in two colours. The large scatter on the amplitudes across the spectrum in the unfiltered data are not present in the filtered data. Such effects of broadband RFI cannot be removed by flagging in the post-processing of data and must be done with a real time filtering.

The amplitude and phase as functions of time for a single baseline after calibration for unfiltered and filtered are shown in the top and middle panels of Fig.24. The effect of filtering is to reduce the scatter along the y-axis in the two plots. Histograms of the calibrated visibility amplitudes in unfiltered and filtered cases are shown in the bottom panels of Fig. 24. The thickness of the tails of the histogram are reduced in the filtered data as can be seen in the reported rms on the peak of 2.5 Jy in unfiltered versus 1.9 Jy in the filtered data.

5.1.2 Visibility amplitude standard deviation

The online RFI excision replaces samples that cross the threshold with digital noise. BB RFI is more correlated for central square baselines as compared to the arm antennas. We expect that the RFI filtering mostly removes the RFI and the effect of replacement by digital noise is very small. However, it may start to affect the actual correlation from the sky. We examined the standard deviations on the calibrated amplitudes of calibrator data as a function of baseline length and quantified the effect when a threshold of 3σ and replacement with digital noise was used for the filtering.

In Fig. 25 the unfiltered and filtered data are shown. For band 3, at short baselines the effect of the filter to reduce the standard deviation on the amplitude is seen. The effect of filtering is less at bands 4 and 5 as these bands are less affected by BB RFI.

We compare the filtering for different bands in Fig. 26. The ratio of standard deviations in unfiltered and filtered data are plotted in serial order from left to right in ascending order of baseline length (also given in the plot). A higher value of the ratio indicates that the standard deviation has improved by that factor. We also have a few points that are just below 1, which means that in those baselines the signal after filtering showed larger standard deviation than the unfiltered. We note that this is limited to less than 2.5% at bands 3, 4 and 5.

5.2   Calibrator flux densities

We compared the calibrator flux densities in order to check for any systematic effect produced by the filtering. Using the task 'visstat' in CASA the flux densities of the calibrators were obtained over about 100 channels (9.7 MHz bandwidth). The calibrated flux densities are within a few percent of those obtained from unfiltered data (Table 3).

5.3   Effect on the flagging percentage

We processed the interferometric data using a pipeline in CASA. The pipeline was used to ensure that the filtered and unfiltered data were analysed in an identical manner. Standard steps of flagging, calibration and imaging were carried out. Self-calibration was carried out to improve the sensitivity. We compared the flagging statistics for the target source in the tests at bands 3 and 4 (Table 4). At short baselines, the flagging is 4% and 6% higher in unfiltered data at bands 3 and 4, respectively. The change in the flagging percentage as a function of uv-distance is shown in Fig. 27. At the short and intermediate length baselines, the percentage of data flagged is lower in the filtered case and comparable on longer baselines.

5.4   Effect on the images

The images from the 1:2 tests carried out in bands 3 and 4 are shown in Figs. 28 and 29. At both the bands there are minor but noticeable differences in the morphology of the extended emission. Qualitatively the appearance of the extended emission is smoother in the filtered image. We also show the images made from baselines shorter than 2 kilolambda (band 3) in Fig. 30. The left and right panels show the images from unfiltered and filtered data respectively on identical colour scale. The fidelity of the image from the filtered data is better as indicated by the contours. The rms in the filtered and unfiltered images are 0.0007 Jy beam^{-1} and 0.0009 Jy beam^{-1}, respectively. The green contours are at ± 0.0014 Jy beam^{-1} and the white contours are at 0.0021 and 0.0042 Jy beam^{-1}.

6   Typical flagging percentages using the RFI counter

The RFI counter was used during the tests to keep track of the percentage of data affected by the filter. The flagging percentage values for the primary calibrator scan for each of the tests are shown in Fig. 31. The typical flagging percentage is $< 5\%$ for Band 2, $< 3\%$ for Band 3, $< 1\%$ for band 4 and $< 0.5\%$ for Band 5.

7   Results at Band 2: De-correlation

At band 2 the data in the frequency range 0.19 - 0.24 GHz were analysed to avoid the regions in the spectrum that were affected by the notch filter and dominant narrow band RFI. The calibrated data towards the primary calibrator are shown in Fig. 32. The trend of reduced standard deviation in the data

15

at short baselines seen at bands 3, 4 and 5 is also seen at band 2. However, there are long baselines that show an increase in the standard deviation after filtering. In Fig. 33, the ratio of standard deviations for band 2 is plotted along with those for the bands 3, 4 and 5. The points with values below 1 indicate those baselines where the scatter has increased after filtering. The origin of this effect is likely the higher flagging percentage that introduces decorrelation in the data.

8   Real-time BB RFI filter : Operational Aspects

The RFI filter operates on 8-bit data, irrespective of the GWB processing bandwidth or the mode of operation. The performance of RFI filter varies under different levels of input power (in presence of strong NB RFI) and it is found that power equalization between 80-100 self counts for GWB is optimal. The power equalization needs to be done in spectral channels void of NB RFI and where the power level is stable and equal. Other recommended settings and the operating procedure for running RFI filtering in GWB is provided in [8] which is available with the GMRT control room. This filter is targeted only to remove BB RFI and hence it may not affect the situation of NB RFI in the filtered data. The flagged fraction for each antenna for the entire observation or for each scan be recorded. The details are available in the SOP. Currently, the command to record this count has to be explicitly entered in the observation command file.

9   Summary and conclusions

The realtime RFI filtering scheme has been implemented for the uGMRT. This scheme is particularly targetted for reducing the impact of broadband RFI on astronomical data. This system was tested by implementing a new testing scheme that allowed to record the filtered and unfiltered data simultaneously. Tests were conducted in the upgrade slots and white slots available in the GMRT observing schedule. The conclusions from the tests and the current status of the system are as follows:

1. The engineering tests show an improvement in signal-to-noise ratio, cross-correlation function, and closure phase.

2. Beam former mode tests towards a standard calibrator show removal of broadband features from the spectrum when the filter is used. Observation of the bright puldar B0329+54 show an improvement by a factor of 4 in the signal-to-noise ratio. Improvements in single pulse detection and frequency-phasogram has also been found.

3. Interferometric mode tests at bands 3, 4 and 5 show that the short baselines (central square) show significantly less number of outliers in amplitude and phases. The calibrator flux densities were recovered within a few percent of the expected value and no systematic was noticed between filtered and unfiltered data.

4. On analysing the filtered and unfiltered data with identical analysis pipeline, it was found that the flagging percentage was reduced in filtered data as compared to unfiltered data by a few to ten percent at bands 3 and 4.

5. Images produced using the filter had improvement in rms and had better image fidelity.

6. An RFI counter also has been implemented and it shows that 5%, 3%, 1% and 0.5% of data samples are replaced by digital noise at bands 2, 3, 4 and 5, respectively.

7. Decorrelation is found to be introduced in filtered data especially at band 2 where the percentage of the RFI is the highest. At bands 3 and 4 the effect of decorrelation is less than 2.5%. We are carrying out further tests to understand the decorrelation.

8. The realtime RFI filtering with 3σ threshold and digital noise replacement has been tested and is released on a shared risk basis from Cycle 38 onwards. A SOP has been written for the control room. In order to use the RFI counter, additional commands need to be added to the command file which can be obtained by writing to us. A short reference document for GTAC users is also written.

9. Further tests to recommend optimal thresholds for different bands are being carried out. Testing for spectral line observations is also being carried out.

Acknowledgements

References

[1] J. M. Ford and K. D. Buch, "RFI Mitigation Techniques in Radio Astronomy," in *2014 IEEE Geoscience and Remote Sensing Symposium*, pp. 231–234, IEEE, 2014.

[2] W. A. Baan, "Implementing RFI mitigation in radio science," *Journal of Astronomical Instrumentation*, vol. 8, 2019.

[3] K. D. Buch, S. Bhatporia, Y. Gupta, S. Nalawade, A. Chowdhury, K. Naik, K. Aggarwal, and B. Ajithkumar, "Towards real-time impulsive RFI mitigation for Radio Telescopes," *Journal of Astronomical Instrumentation*, vol. 5, no. 04, p. 1641018, 2016.

[4] K. D. Buch, K. Naik, S. Nalawade, S. Bhatporia, and Y. Gupta, "Implementing and Characterizing Real-Time Broadband RFI Excision System for the GMRT Wideband Backend," *IETE Technical Review*, pp. 1–9, 2018.

[5] G. Swarup, "Power-line Radio Frequency Interference at the GMRT," *NCRA Technical Report R233*, vol. -, Sept 2008.

[6] G. Swarup, "Identification of Radio Frequency Interference (RFI), its Characteristics and Mitigation to Optimize Performance of the GMRT," *Technical Report*, vol. -, 14th July 2014.

[7] K. D. Buch, K. Naik, S. Nalawade, S. Bhatporia, Y. Gupta, and B. Ajithkumar, "Real-time implementation of MAD-based RFI Excision on FPGA," *Journal of Astronomical Instrumentation*, vol. 8, 2019.

[8] K. D. Naik and K. D. Buch, "Running Broadband RFI Filtering on GWB-IV," *GMRT*, vol. 6, June 2018.
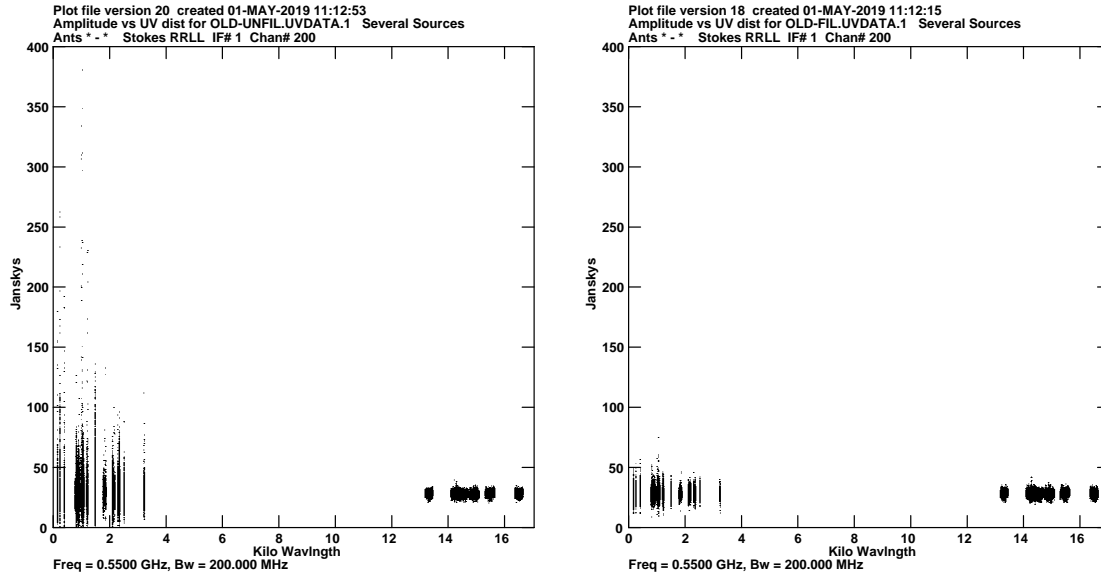
Figure 21: Band 4, 14 June 2018: Calibrated amplitude versus uv-distance is shown for the unfiltered (left) and filtered (right) data for channel 200 (0.550 GHz). The short baselines where the BB RFI is known to be correlated shows significant improvement. [Sec. 5.1]

Table 3: Summary of calibrator flux densities in filtered and unfiltered data. [Sec. 5.2]

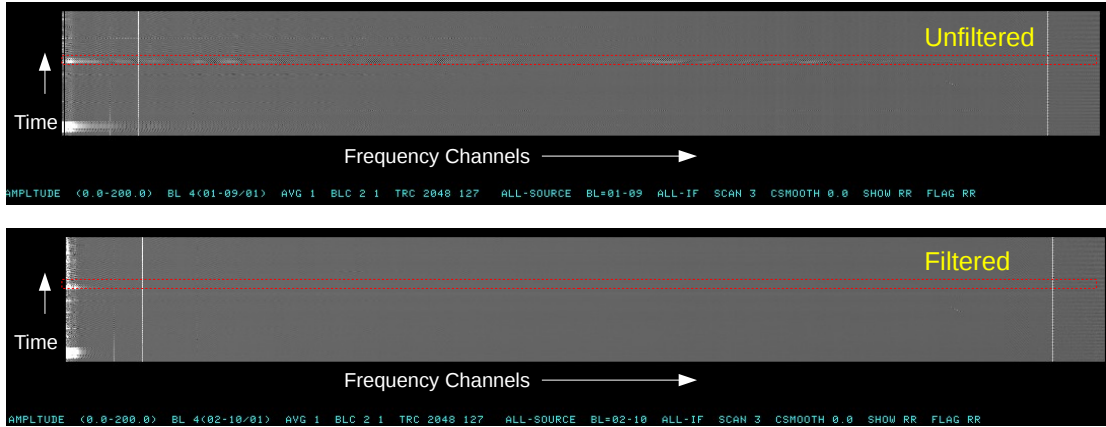| Date	Band	Mode	Source	Un-filtered Jy	Filtered Jy	Fractional change (%)
14 Jun. 2018	4	1:2	3C48	34.3 ± 0.2	33.6 ± 0.1	2
11 Aug. 2019	3	1:2	3C48	38.2 ± 3.6	38.1 ± 2.9	0.3
			0116-208	10.0 ± 2.0	9.7 ± 1.3	3.0
13 Aug. 2019	4	1:2	3C48	30.6 ± 3.3	30.6 ± 3.2	0
			0116-208	7.8 ± 0.9	7.9 ± 0.9	1.2
09 Sept. 2019	5	1:2	3C147	22.6 ± 3.0	22.5 ± 3.0	0.4

Figure 22: Band 4, 14 June 2018: Time-frequency plane for the baseline C00-C09 in unfiltered (C01-C10 in filtered) is shown on the same grey-scale ranging from 0 - 200 Jy. A broadband feature is marked with a box in both unfiltered and filtered data. [Sec. 5.1]

Table 4: Summary of flagging on target source.[Sec. 5.3]

Band	Unfiltered Flagged (%) < 2klambda	Filtered Flagged (%) < 2klambda	Unfiltered Flagged (%) all uvrange	Filtered Flagged (%) all uvrange
3	40.2	36.1	53.7	53.7
4	15.0	9.1	33.6	32.7
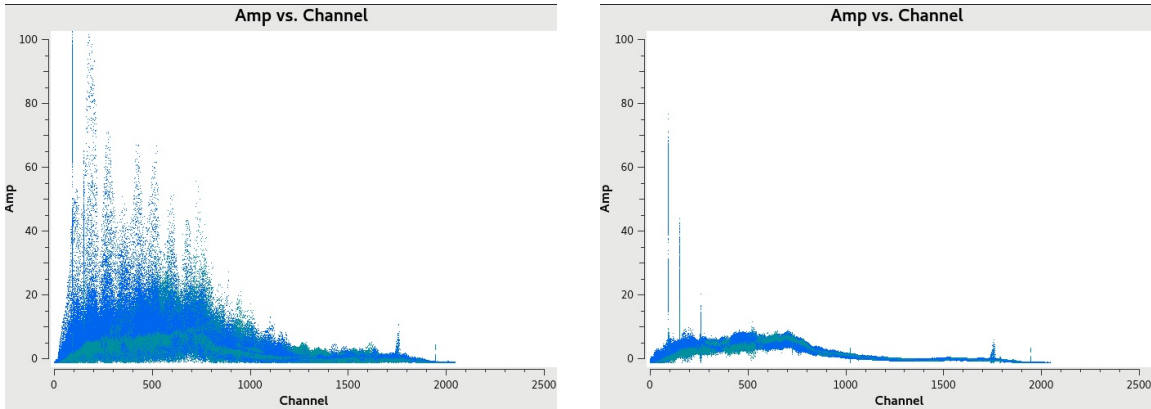
Figure 23: Band 4, 14 June 2018: The uncalibrated spectrum of the baseline C00-C02 in unfiltered data is shown in the left column (filtered copy C01-C03 in the right column). The LL polarization is shown in blue and RR in green. [Sec. 5.1]

19
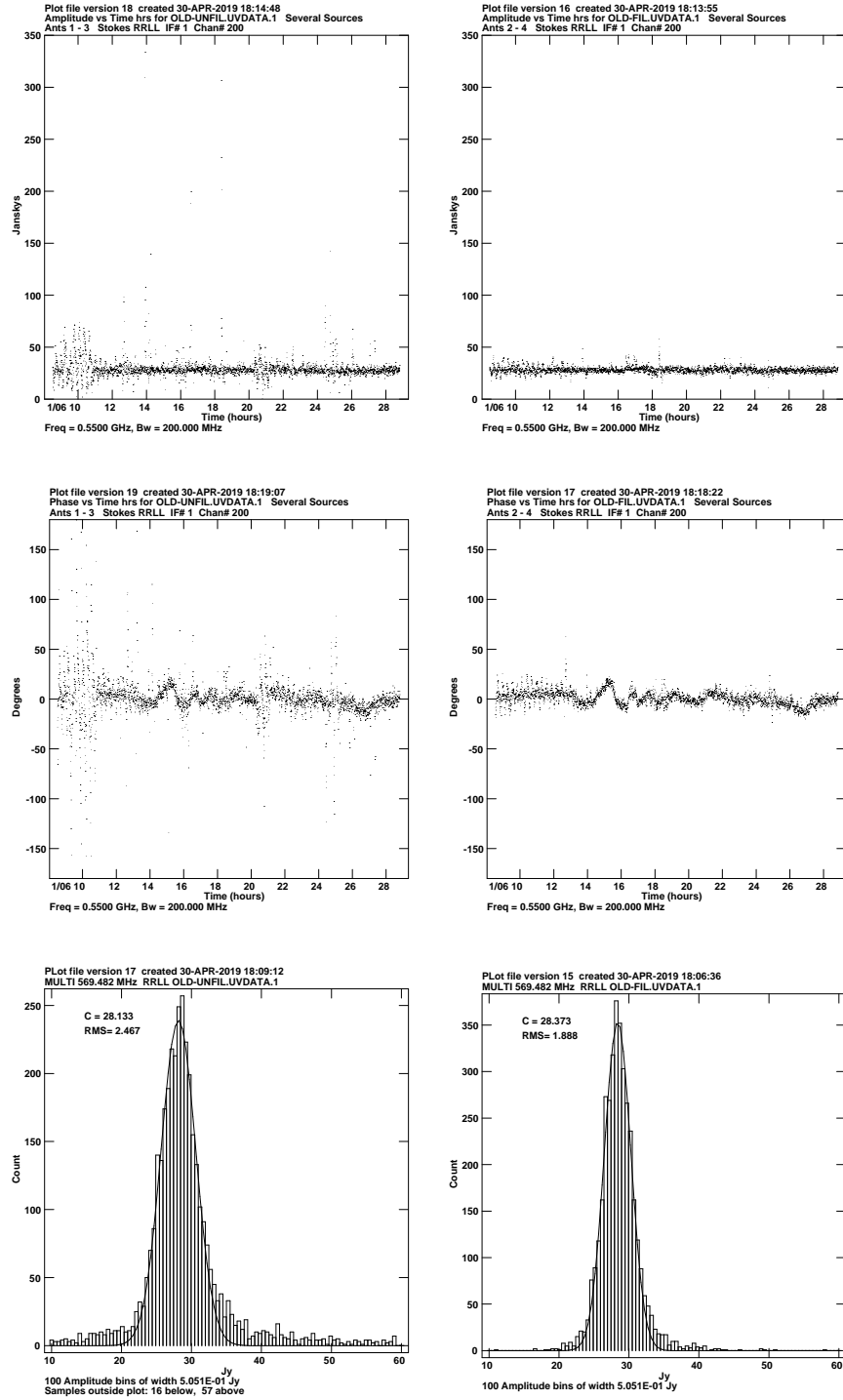
Figure 24: Band 4, 14 June 2018: The baseline C00-C02 in unfiltered data is shown in the left column (filtered copy C01-C03 in the right column) for the channel 200. The top panels show Amplitude Vs time and the middle panels show Phase Vs Time. The bottom panels show the histograms of the amplitudes with a Gaussian fit for unfiltered and filtered data. [Sec. 5.1]
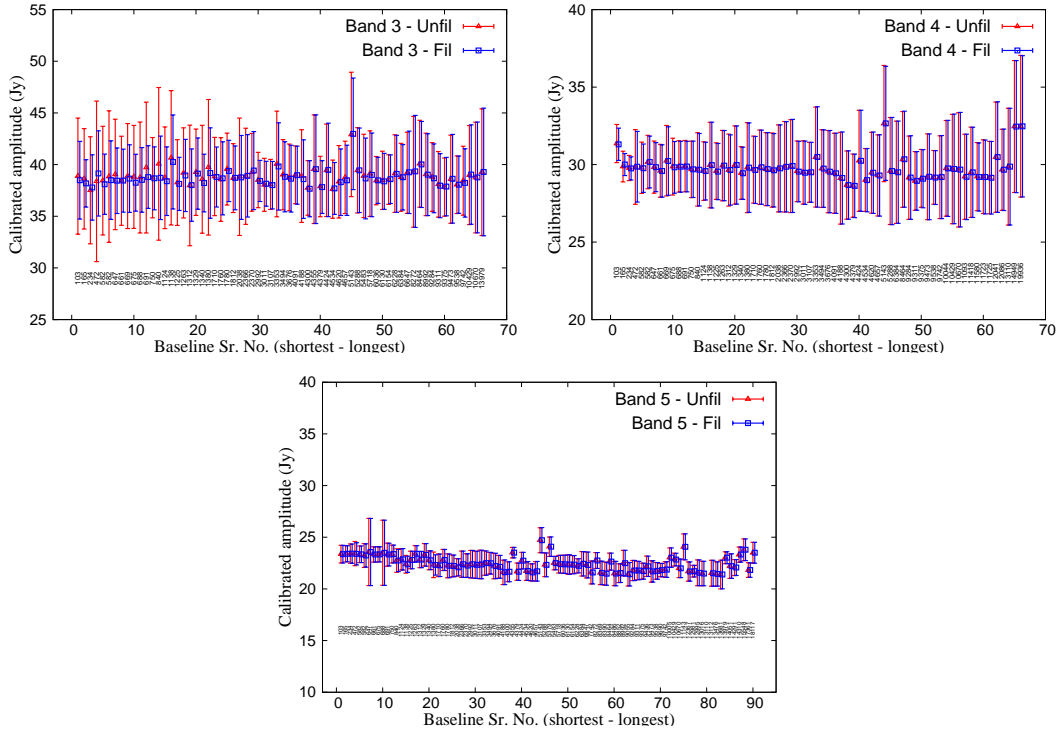
Figure 25: The calibrated flux density of a primary calibrator source for a single channel is plotted as a function of baseline numbers sorted according to their lengths. The integers in the plot indicate the length of the baseline in metres ranging from 100 m to 14, 20 and 15.5 km for bands 3, 4 and 5 respectively. The unfiltered (red) and filtered (blue) points are offset on the x-axis for comparison. [Sec. 5.1]
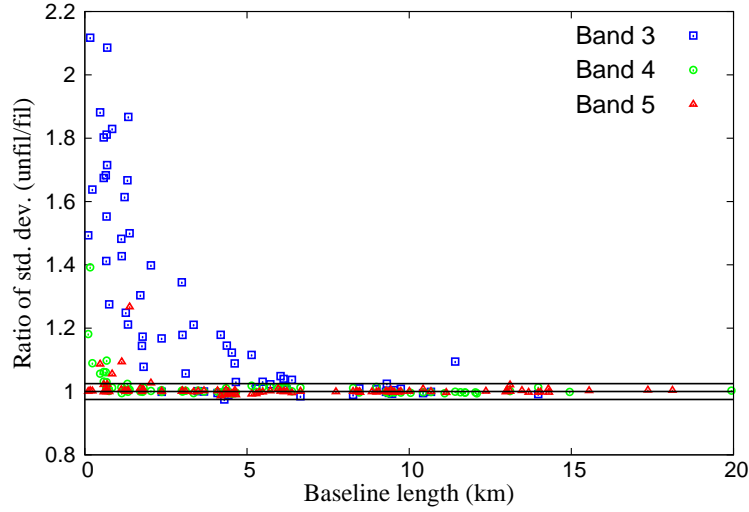
21

Figure 26: The ratio of standard deviations on the visibility amplitude (unfiltered/filtered) versus baseline length is shown. At short baselines there is considerable improvement and at long baselines it is close to 1. This quantity is plotted for bands 3, 4 and 5. For a few baselines the filtered standard deviation is larger than that of unfiltered - this is confined to less than 2.5%. The horizontal lines are at 1.0, 1.025 and 0.975. [Sec. 5.1]
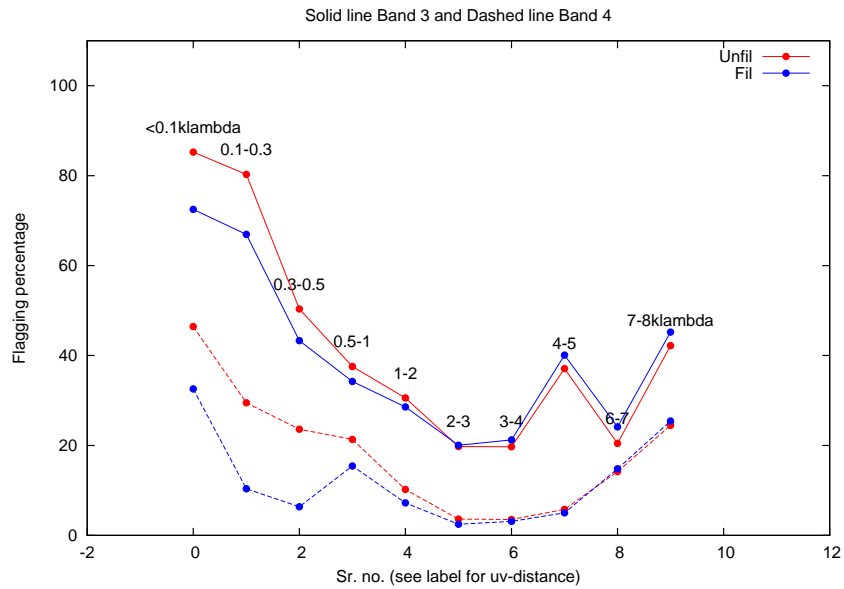

Figure 27: Flagging percentage versus baseline serial numbers sorted according to their length are shown for bands 3 (solid) and 4 (dashed) using red colour for unfiltered data and blue for filtered data. The points are obtained in uv-distance bins as labelled in above the points. [Sec. 5.3]
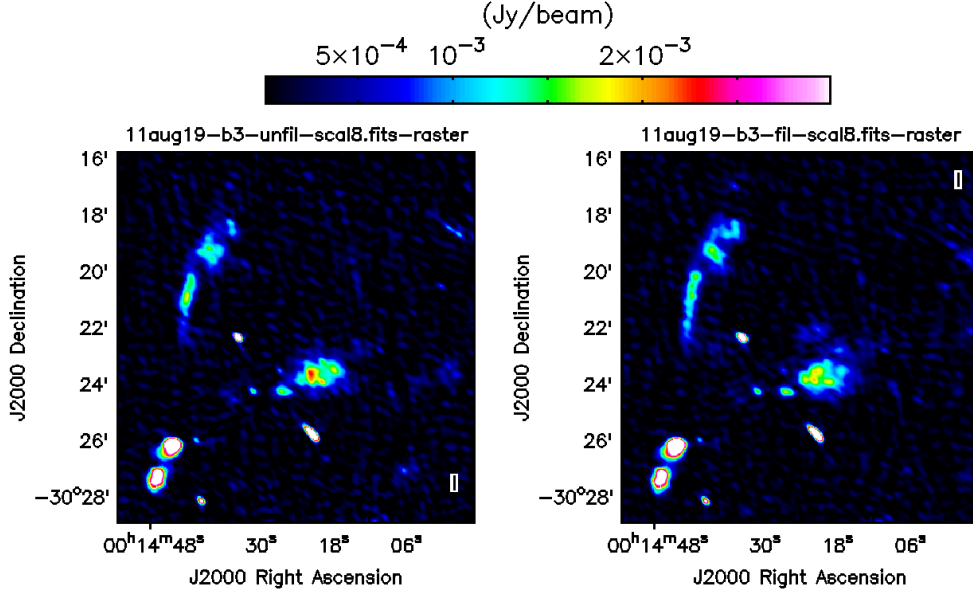
Figure 28: Band 3 images of A2744 field: unfiltered (left) and filtered (right). The rms in the unfiltered image is 115 μJy beam^{-1} and in the filtered image is 107 μJy beam^{-1}. The beam size is $17.9'' \times 10.6''$, position angle 53°. The morphology of the extended emission has a smoother distribution in the filtered data as compared to the unfiltered data. [Sec. 5.3]
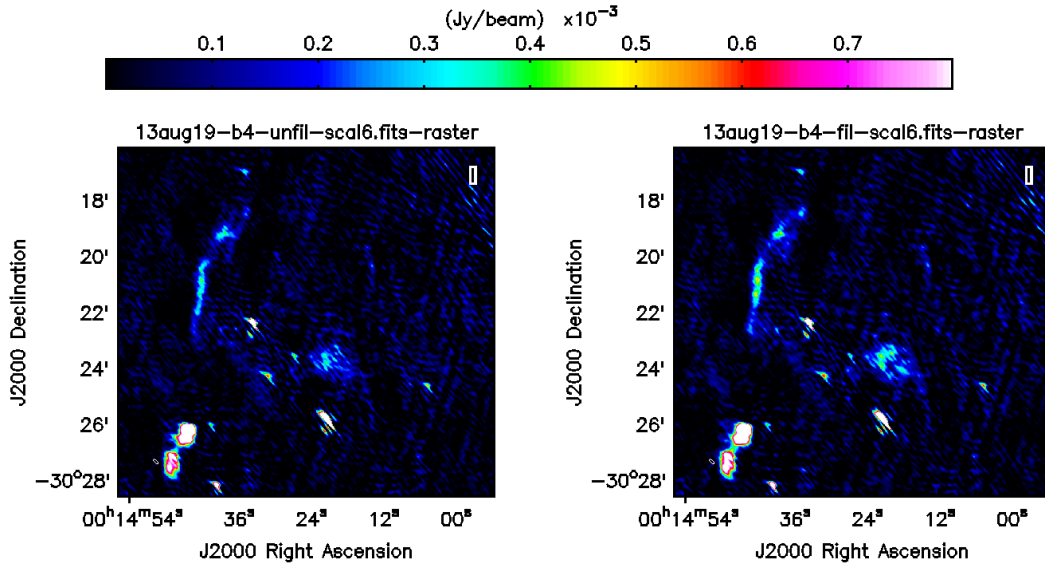

Figure 29: Band 4 images of A2744 field: unfiltered (left) and filtered (right). The rms in the unfiltered image is 44 μJy beam^{-1} and in the filtered image is 42 μJy beam^{-1}. The beam size is $14.5'' \times 4.9''$, position angle 45.7°. [Sec. 5.3]
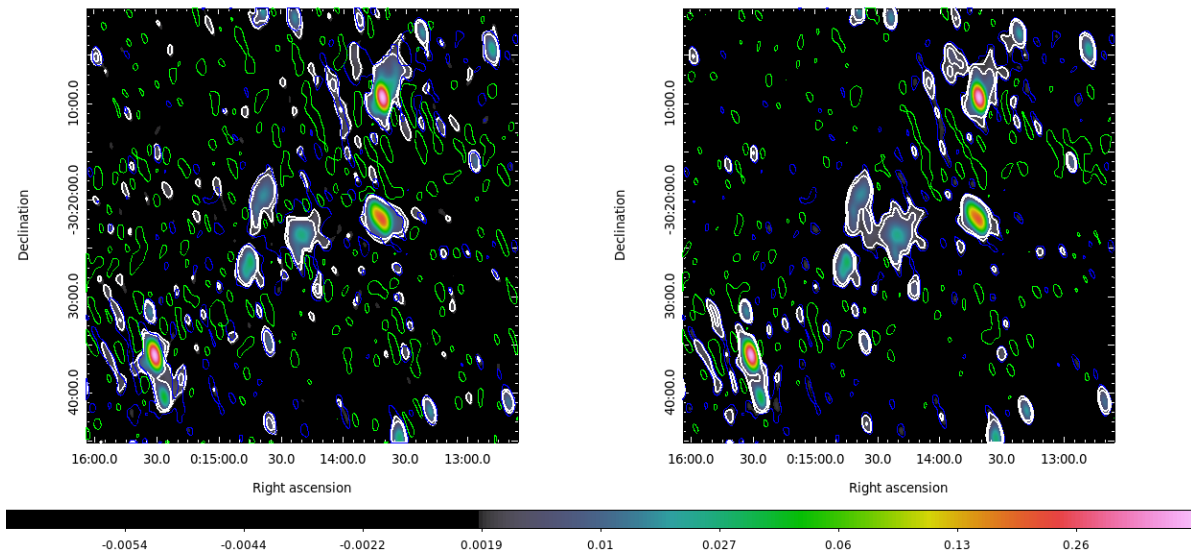
Figure 30: Image of A2744 made with use of baslines < 2klambda at band 3 using unfiltered data (left) and filtered data (right). The contours are drawn at identical levels in the two panels. The green contours are at -0.0014, blue are at 0.0014 Jy beam^{-1}. This represents a level of 2σ where σ is the rms in the filtered image. The white contours are at 0.0021 and 0.0042 Jy beam^{-1} and represent 3 and 6 σ levels. The coordinates and the colour scale (Jy beam^{-1}) are matched in the two panels. [Sec. 5.3]
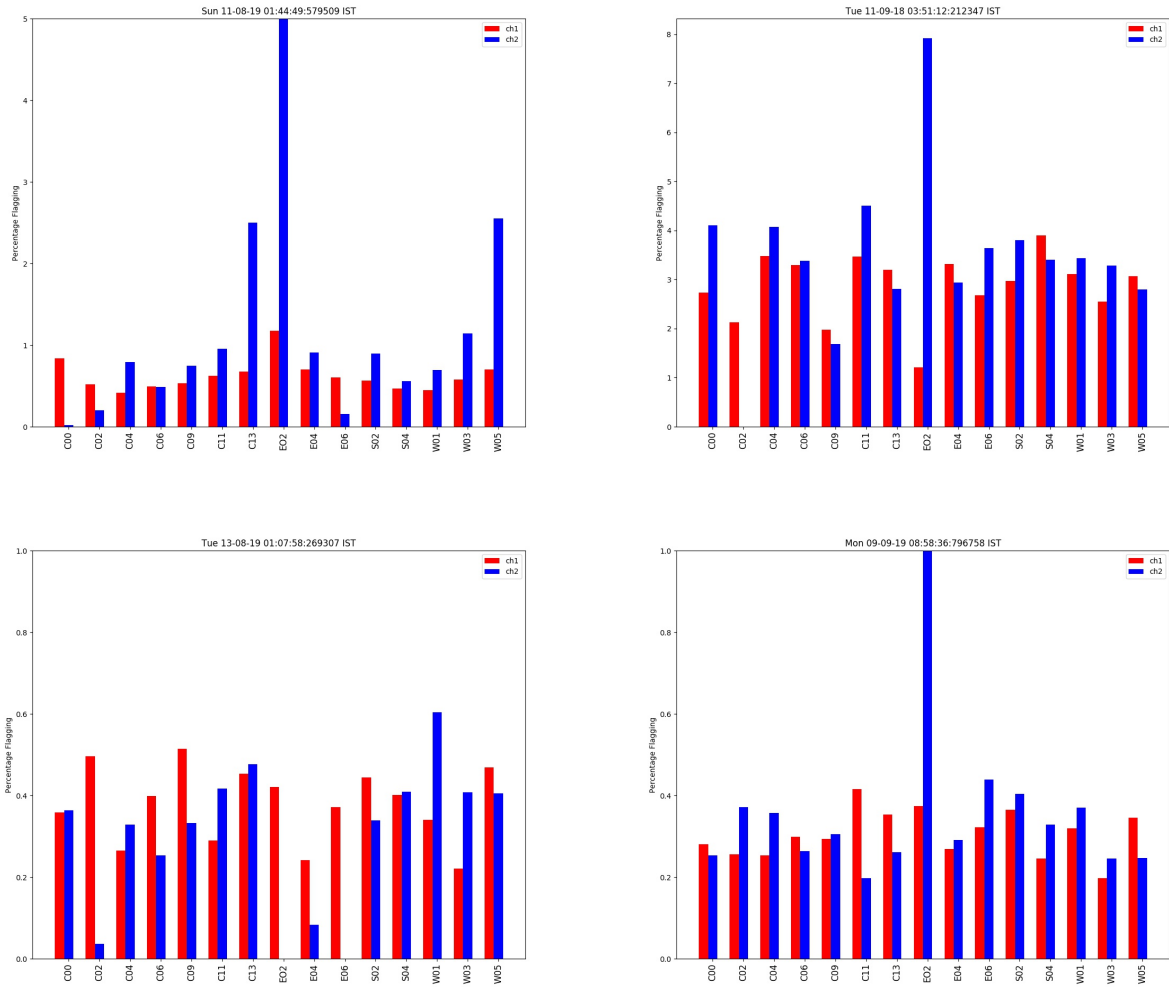
Figure 31: Band 2, 11 Sep. 2018, Band 3, 11 Aug. 2019, Band 4, 13 Aug. 2019 and Band 5, 09 Sep. 2019 counter histograms are shown. The two polarizations are shown in red (Channel 1) and blue (Channel 2) colour. The E02 antenna (channel-2) counts have a problem at all bands for one polarization. The typical flagging percentage is $< 5\%$ for Band 2 (top-right), $< 3\%$ for Band 3 (top-left), $< 1\%$ for band 4 (bottom-left) and $< 0.5\%$ for Band 5 (bottom-right). [Sec. 6]
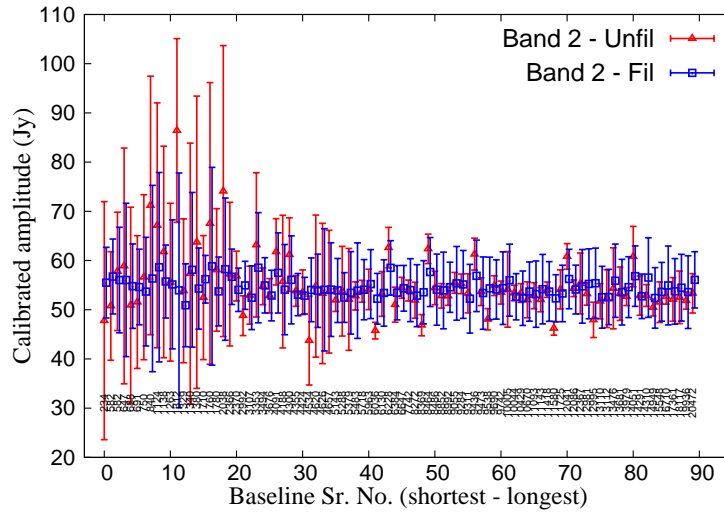
Figure 32: The band 2 calibrated flux density of a primary calibrator source for a single channel is plotted as a function of baseline numbers sorted according to their lengths. The integers in the plot indicates the length of the baseline in metres. The unfiltered (red) and filtered (blue) points are offset on the x-axis for comparison. [Sec. 7]
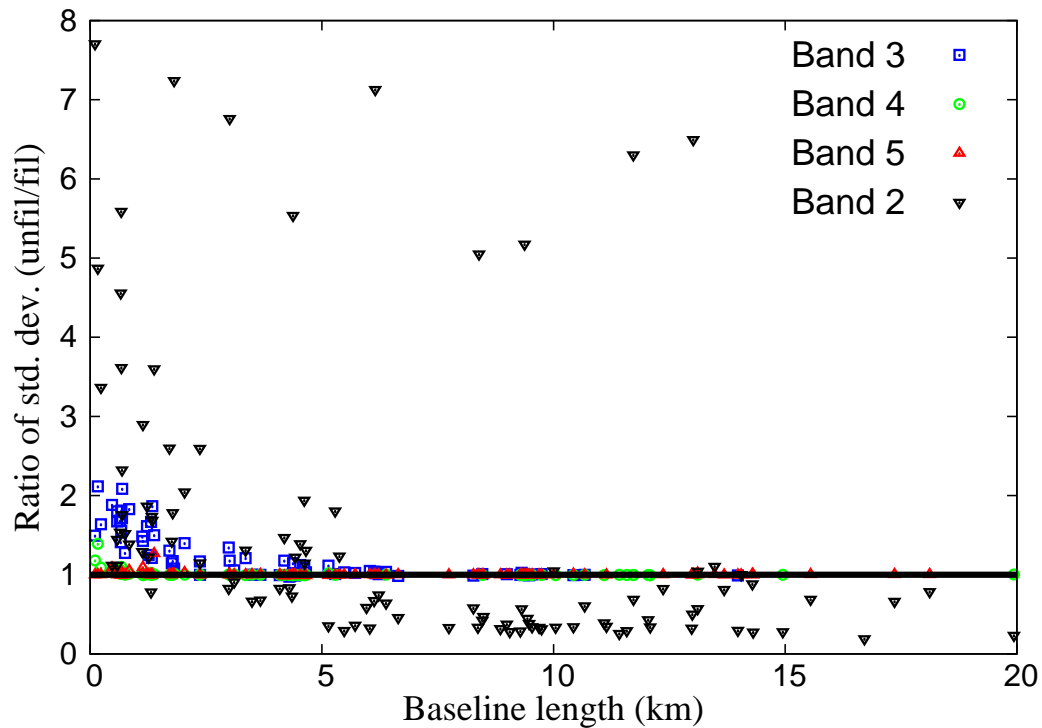

Figure 33: The ratio of standard deviations on the visibility amplitude (unfiltered/filtered) versus baseline length is shown for band 2 in black and the remaining points are plotted from Fig. 26. [Sec. 7]